quantum reports

MDPI

Article

Hybrid Quantum-Classical Eigensolver Without Variation or Parametric Gates

Pejman Jouzdani * and Stefan Bringuier

General Atomics, San Diego, CA 92121, USA; Stefan.Bringuier@ga.com
* Correspondence: jouzdanip@fusion.gat.com

Abstract: The use of near-term quantum devices that lack quantum error correction, for addressing quantum chemistry and physics problems, requires hybrid quantum-classical algorithms and techniques. Here, we present a process for obtaining the eigenenergy spectrum of electronic quantum systems. This is achieved by projecting the Hamiltonian of a quantum system onto a limited effective Hilbert space specified by a set of computational bases. From this projection, an effective Hamiltonian is obtained. Furthermore, a process for preparing short depth quantum circuits to measure the corresponding diagonal and off-diagonal terms of the effective Hamiltonian is given, whereby quantum entanglement and ancilla qubits are used. The effective Hamiltonian is then diagonalized on a classical computer using numerical algorithms to obtain the eigenvalues. The use case of this approach is demonstrated for ground state and excited states of BeH_2 and LiH molecules, and the density of states, which agrees well with exact solutions. Additionally, hardware demonstration is presented using IBM quantum devices for H_2 molecule.

Keywords: quantum computing; quantum algorithms; quantum chemistry

Citation: Jouzdani, P.; Bringuier, S. Hybrid Quantum-Classical Eigensolver Without Variation or Parametric Gates. *Quantum Rep.* **2021**, *3*, 137–152. https://doi.org/10.3390/quantum3010008

Academic Editor: Henry Chermette
Received: 13 January 2021
Accepted: 27 January 2021
Published: 31 January 2021

1. Introduction

Quantum computers offer the ability to address problems in quantum many-body chemistry and physics by quantum simulation or in a hybrid quantum-classical approach. The latter method is considered the most promising approach for noisy-intermediate scale quantum (NISQ) devices [1]. The prospect and benefits of quantum algorithms, along with suitable hardware, is in overcoming the complexity of the wave-function of a quantum system as it scales exponentially with system size [2]. Therefore, developing techniques and algorithms for NISQ era devices that may prove to have some computational advantage themselves, or establish a path towards ideas and foundations that provide advantage for future error-corrected quantum devices, is a worthwhile pursuit.

The leading algorithms intended to be executed on NISQ devices, which aim to determine solutions to an electronic Hamiltonian, are variational in nature [3]. One specific algorithm is the variational quantum eigensolver (VQE), which has been tremendously successful in addressing chemistry and physics problems on quantum hardware and NISQ devices [4–12]. However, the restriction or challenge that exist with VQE is the need for prior insight with regard to selecting the trial quantum state, i.e., ansatz circuit. Furthermore, the classical optimization of the ansatz parameters may be a poorly converging problem [13,14], therefore limiting the applicability of VQE for obtaining results accurate enough for chemical or physical interpretation. Finally, the realization of ansatz circuits that are motivated by domain knowledge, for example, the unitary coupled cluster ansatz for chemistry problems [15], may not be directly applicable on NISQ hardware, therefore requiring clever modification to obtain hardware efficient ansätze [6,7,16].

In this work, we present a pragmatic hybrid quantum-classical approach for calculating the eigenenergy spectrum of a quantum system within an effective model. Firstly, an effective Hamiltonian is obtained through measurement of short-depth quantum circuits. The effective Hamiltonian is essentially the projection of the quantum system Hamiltonian

onto a limited set of computational bases. The basis set is prepared with the intent of ensuring the dimensions of the corresponding matrix does not grow exponentially with the system size. In order to evaluate the matrix elements of the effective Hamiltonian, suitable non-parametric quantum circuits are specified. The quantum circuits are designed, executed, and measured. From the result of the measurements, the diagonal and off-diagonal terms of the effective Hamiltonian matrix are obtained. On the classical side, the effective Hamiltonian matrix, with suitable dimensions, is diagonalized numerically using a classical computer.

The paper is organized as follows: A short background is presented in Section 2. In Section 3, the steps taken in our hybrid quantum-classical approach are explained in detail. In Section 4, we demonstrate the application of this hybrid approach on simple chemical molecules BeH_2 and LiH. In Section 5, the approach is demonstrated on the IBMQ 5-qubit Valencia quantum processor [17] for H_2 molecule. Finally, we discuss the integration of VQE and the proposed approach in Section 6.

2. Background

Consider a quantum many-body system of electrons with the second quantized Hamiltonian:

$$\hat{H} = \sum_{ij} \kappa_{ij} a_i^\dagger a_j + \sum_{ijkl} v_{ijkl} a_i^\dagger a_j^\dagger a_k a_l. \tag{1}$$

$a_i^\dagger$ and a_i are the creation and annihilation operators, respectively. The anticommutator for the creation and annihilation are given by: $a_i a_j^\dagger + a_j^\dagger a_i = \delta_{ij}$ and $a_i a_j + a_j a_i = a_i^\dagger a_j^\dagger + a_j^\dagger a_i^\dagger = 0$. These rules enforce the non-abelian group statistics for fermions, that is, under exchange of two fermions the wave-function yields a minus sign.

The indices in Equation (1) refer to single-electron states. The coefficients κ_{ij} and v_{ijkl} are the matrix integrals

$$\kappa_{ij} = \langle i|\hat{K}_1|j\rangle \tag{2}$$

and

$$v_{ijkl} = \langle ij|\hat{V}_{12}|kl\rangle, \tag{3}$$

where $\hat{K}_1$ and $\hat{V}_{12}$ operators correspond to one- and two-body interactions respectively. Since $\hat{K}_1$ and $\hat{V}_{12}$ can depend on other parameters, such as the distance between nuclei, the Hamiltonian in Equation (1) represents a class of problems. However, this class of problems has the common property that the number of fermions is a conserved value. Strictly speaking, the terms in the Hamiltonian act on fixed-particle-number Hilbert spaces, $\mathcal{H}_{N_F}$, that have the correct fermionic antisymmetry, with N_F denoting the number of electrons. In this paper, we consider this class of electronic systems where the Hamiltonian is assumed to be in the form of Equation (1). The coefficients expressed in Equations (2) and (3) can be obtained using software packages developed for quantum chemistry calculations that perform efficient numerical integration [18].

Mapping to Qubits & Computational Basis

The Hamiltonian as written in Equation (1) can be expressed in the form of qubit operations (i.e., Pauli matrices). This requires a transformation that preserves the anti-commutation of the annihilation and creation operators. One transformation that satisfies the criteria, and is based on the physics of spin-lattice models, is the Jordan-Wigner (JW) transformation [19]. The JW-transformed Hamiltonian takes the form

$$\hat{H} = \sum_s \lambda_s \hat{h}_s, \tag{4}$$

in which λ_s's are scalar and a *Pauli string* operator $\hat{h}_s$ is defined as

$$\hat{h}_s = \hat{O}_1^s \otimes \cdots \otimes \hat{O}_N^s. \tag{5}$$

$\hat{O}_i^s \in \{\hat{I}, \hat{X}, \hat{Y}, \hat{Z}\}$ acts on the i-th qubit, $\{\hat{X}, \hat{Y}, \hat{Z}\}$ are the three Pauli matrices [20], and $\hat{I}$ is the identity matrix with the number of qubits denoted as N.

If the number of $\hat{I}$ operators in the tensor product of $\hat{h}_s$ is $N-k$, we call $\hat{h}_s$ a k-local Pauli string operator. Upon the JW transformation of the Hamiltonian, a Fock basis of the second quantization representation is in one-to-one correspondence with a computational basis of the qubits [21]. In other words, a computational basis of

$$|\mathbf{n}\rangle = |n_0, n_1, \ldots, n_N\rangle, \tag{6}$$

with N qubits, where $n_i \in \{0, 1\}$, is equivalent to a an antisymmetric Fock basis.

Within the finite, but exponentially large, Hilbert space spanned by 2^N computational basis set, an effective matrix representation of the Hamiltonian may be possible, specifically, if one can efficiently evaluate the matrix elements $\langle \mathbf{n}'|\hat{H}|\mathbf{n}\rangle$ for an arbitrary computational basis $|\mathbf{n}\rangle$ and $|\mathbf{n}'\rangle$. Furthermore, assuming that the dimensions of the resulting effective matrix are relatively small, the matrix can be diagonalized on a classical computer, where its eigenvalues approximate the spectrum of the original Hamiltonian.

In this paper, we show how to evaluate a matrix element $\langle \mathbf{n}'|\hat{H}|\mathbf{n}\rangle$ for arbitrary computational basis $|\mathbf{n}\rangle$ and $|\mathbf{n}'\rangle$, using a quantum circuit that has a circuit depth $\mathcal{O}(N)$. We do so by using ancilla qubits; thus, $N+1$ physical resources are needed. In addition, we discuss how to choose an effective subspace for a given electronic Hamiltonian, with a dimension N_s, based on physical motivations (see Section 3.3). The condition $N_s << 2^N$ makes it possible to diagonalize the Hamiltonian on a classical computer. In Section 4, we numerically demonstrate this method for simple quantum chemistry systems, focusing on ground state energy and the density of state calculations of the low-energy spectrum. Furthermore, in Section 5 we use the IBMQ 5-qubit Valencia device to measure the terms for H_2 in the complete computational basis of 4 qubits.

3. Constructing an Effective Matrix Representation for a Hamiltonian by Qubit Measurement

3.1. Effective Hamiltonian and Circuit Representation

We first consider a Hamiltonian $\hat{H}$ that is expressed in terms of Pauli strings as in Equation (4). Additionally, a subspace $\mathcal{S} = \{|\mathbf{n}\rangle\}$, with N_s corresponding computational bases, is considered such that $N_s << 2^N$. Let us define the *effective Hamiltonian* matrix as the projection of $\hat{H}$ onto this subspace; that is

$$\hat{H}_{eff} = \sum_{\mathbf{n},\mathbf{n}' \in \mathcal{S}} \langle \mathbf{n}|\hat{H}|\mathbf{n}'\rangle \; |\mathbf{n}\rangle\langle \mathbf{n}'|. \tag{7}$$

The next step is to define a simple quantum circuit that utilizes one ancillary qubit to measure $\langle \mathbf{n}|\hat{H}|\mathbf{n}'\rangle$ matrix element.

The dimension of $\hat{H}_{eff}$ depends on the choice of the subspace in $\mathcal{S}$. The choice of the subspace, intuitively, depends on the physics of the problem. However, the focus of this paper is towards quantum chemistry problems, which are a primary application for NISQ devices. For this class of Hamiltonians, there is a systematic way to select the appropriate subspace. This is discussed in Section 3.3.

The evaluation of diagonal terms in $\hat{H}_{eff}$, e.g., $\langle \mathbf{n}|\hat{H}|\mathbf{n}\rangle$, is trivially performed by preparing N qubits as a bit string of $|\mathbf{n}\rangle \equiv (n_0, \ldots, n_N)$ and measuring $\hat{H}$. The measurement of the total Hamiltonian is obtained by measuring every individual Pauli string, $\hat{h}_s$, in Equation (5). The diagonal terms are then given by

$$\langle \mathbf{n}|\hat{H}|\mathbf{n}\rangle = \sum_s \lambda_s \langle \mathbf{n}|\hat{h}_s|\mathbf{n}\rangle. \tag{8}$$

The off-diagonal matrix elements, e.g., $\langle \mathbf{n}'|\hat{H}|\mathbf{n}\rangle$, which are generally complex numbers, can be evaluated using a single ancillary qubit. This can be done by considering the quantum circuits as shown in Figure 1. The two circuits shown in Figure 1a,b are used to calculate the real and imaginary parts of the matrix element, respectively. In both circuits, the $N+1$ qubits are initially prepared in $|\psi_{int}\rangle = |0\rangle \otimes |0\rangle^{\otimes N}$ state. The qubits are assumed to be enumerated linearly from 1 to $N+1$, where the $N+1$-th qubit is the control qubit.

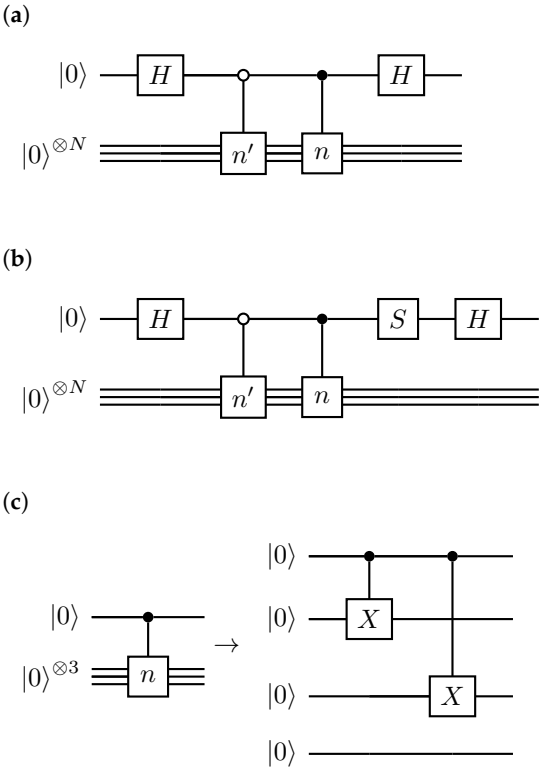

Figure 1. Quantum circuits for measuring (**a**) the *real* and (**b**) *imaginary* parts of an off-diagonal element $\langle \mathbf{n}'|\hat{H}|\mathbf{n}\rangle$. (**c**) A controlled-$n$ gate represents a set of CNOT gates that prepares the qubits in the state $|n\rangle$. An example of controlled-n for $N = 3$ and $|n\rangle = |011\rangle$ is shown.

After applying the first Hadamard gate on the ancillary qubit, from left to right as shown in the circuits in Figure 1a,b, the quantum state of all the qubits is

$$|\psi\rangle = \frac{1}{\sqrt{2}}\Big[|0\rangle|0\rangle^{\otimes N} + |1\rangle|0\rangle^{\otimes N}\Big], \tag{9}$$

which, after a sequence of controlled-X gates, becomes entangled as

$$|\psi\rangle = \frac{1}{\sqrt{2}}\big[|0\rangle|\mathbf{n}'\rangle + |1\rangle|\mathbf{n}\rangle\big]. \tag{10}$$

Here, control gates (controlled-n and controlled-n') flip N_F qubits (corresponding to the N_F occupied electronic states) and prepare the target qubits in the computational basis $|\mathbf{n}\rangle$ ($|\mathbf{n}'\rangle$), conditioned on the state of the control qubit is $|1\rangle$ ($|0\rangle$).

An example of a controlled-n gate that prepares target qubits in $|011\rangle$ state is shown in Figure 1c. In practice, this part of the circuit requires two-qubit gates (e.g., CNOT) and perhaps the need for full connectivity of qubits in order to operate on any two qubits. Full connectivity of qubits could potentially be realized with ion-trapped devices [22]. See Section 6 for further discussion.

Depending on whether the *real part* or the *imaginary part* is calculated, the last gate acting on the control qubit changes. With regard to the *real part*, after applying the last Hadamard gate on the control qubit in Figure 1a, the quantum state is

$$|\psi\rangle = \frac{1}{2}|0\rangle\left[|\mathbf{n}'\rangle + |\mathbf{n}\rangle\right] + \frac{1}{2}|1\rangle\left[|\mathbf{n}'\rangle - |\mathbf{n}\rangle\right]. \tag{11}$$

Using this prepared quantum state, one can measure

$$\hat{M}_0 \quad = \quad |0\rangle\langle 0| \otimes \hat{H} \tag{12}$$

at the end of the circuit and have

$$\begin{aligned} m_0 &= \langle\psi|\left[|0\rangle\langle 0| \otimes \hat{H}\right]|\psi\rangle \\ &= \frac{1}{2^2}\left(\langle\mathbf{n}|\hat{H}|\mathbf{n}\rangle + \langle\mathbf{n}'|\hat{H}|\mathbf{n}'\rangle + 2\mathbf{Re}\left[\langle\mathbf{n}|\hat{H}|\mathbf{n}'\rangle\right]\right). \end{aligned} \tag{13}$$

Thus, after substituting for the diagonal elements $\langle\mathbf{n}|\hat{H}|\mathbf{n}\rangle$ and $\langle\mathbf{n}'|\hat{H}|\mathbf{n}'\rangle$, using Equation (8), one obtains the real part of the off-diagonal matrix element $\langle\mathbf{n}|\hat{H}|\mathbf{n}'\rangle$. The value m_0 in Equation (13) is measured on a quantum device using the identity $|0\rangle\langle 0| = \frac{1}{2}(\hat{I} + \hat{Z})$, by

$$\begin{aligned} m_0 &= \frac{1}{2}\langle\psi|\hat{I} \otimes \hat{H}|\psi\rangle + \frac{1}{2}\langle\psi|\hat{Z} \otimes \hat{H}|\psi\rangle \\ &= \sum_s \frac{\lambda_s}{2}\langle\psi|\hat{I} \otimes \hat{h}_s|\psi\rangle + \frac{\lambda_s}{2}\langle\psi|\hat{Z} \otimes \hat{h}_s|\psi\rangle. \end{aligned} \tag{14}$$

The *imaginary part* can be obtained in a similar fashion as done for the *real part*, but with a slight modification to the circuit as shown in Figure 1b. The key addition is a phase-gate, S, before the execution of the last Hadamard gate on the control qubit. This yields the quantum state

$$|\psi\rangle = \frac{1}{2}|0\rangle\left[|\mathbf{n}'\rangle + i|\mathbf{n}\rangle\right] + \frac{1}{2}|1\rangle\left[|\mathbf{n}'\rangle - i|\mathbf{n}\rangle\right] \tag{15}$$

that now includes a phase factor i before $|n\rangle$. After the last Hadamard gate in Figure 1b, and following the same steps, Equations (12)–(14), the imaginary part $\mathbf{Im}\left[\langle\mathbf{n}|\hat{H}|\mathbf{n}'\rangle\right]$ is obtained.

Our approach differs from the typical hybrid quantum-classical paradigm used in ground state chemistry electronic structure calculations in that the quantum hardware is used as a coprocessor to measure these matrix elements. Therefore, no parameterized ansatz or variational optimization is required. In this approach, the depth of the quantum circuit is significantly reduced; however, our method is based on the assumption that the dimensions of $\hat{H}_{eff}$ in Equation (7) are reasonable enough such that it can be diagonalized using classical numerical algorithms.

3.2. Implementing Measurements

As shown in Equation (14), the expectation value of the Hamiltonian becomes the weighted sum of expectations for the set of Pauli string operators with respect to the output quantum state of the circuit. Since these operators are not in general commuting, one needs to setup and run a number of different quantum circuits. This number can be up-to all Pauli string operators in the Hamiltonian. Each circuit is then executed many times and every time the qubits are measured, the results are realized in different computational bases. The sampled realization provides a probability distribution and is used to estimate the expectation value of the Pauli string.

Generally, measurements are done either directly or indirectly. In the case of direct measurements, single-qubit rotations are applied to a subset of qubits at the end of the circuit. This subset is identified based on the locations in the tensor-product of the operator $\hat{h}_s$ that are not identity $\hat{I}$. This set of rotations essentially changes the computational bases in which the given operator $\hat{h}_s$ is diagonal. The direct measurement is commonly used in the experimental demonstration of quantum hardware and VQE [6].

The indirect measurement approach [23] requires a series of controlled gates that are applied to the N target qubits, using one ancillary control qubit. The indirect measurement method is used in iterative quantum phase estimation algorithms [24].

Although the two types of measurement approaches are theoretically equivalent [20], experimentally, there are differences. The benefits and drawbacks of direct and indirect measurements are discussed, for example, in Reference [25]. The main difference is the number of times the circuit is to be executed to achieve a desired precision ϵ, which is $\mathcal{O}(\frac{1}{\epsilon^2})$ and $\mathcal{O}(\frac{1}{\epsilon})$ for direct and indirect measurements respectively. The implementation of a general control-U gate in the indirect measurement is a challenging task [23]. However, in regards to our purposed approach, where the U operator is a single Pauli string, the indirect measurement implementation is straightforward.

The indirect measurement can be adapted as shown in quantum circuit in Figure 2. An additional control qubit is added to this circuit. The Pauli operators are applied on the k locations of $\hat{h}_s$ when the control is in state $|1\rangle$. It is straightforward to follow the quantum state of the qubits throughout the circuit. The final state reads as:

$$|\psi\rangle = \frac{1}{2}|00\rangle\Big[|\mathbf{n}'\rangle + |\mathbf{n}\rangle + \hat{h}|\mathbf{n}'\rangle + \hat{h}|\mathbf{n}\rangle\Big] + \dots. \tag{16}$$

Upon measuring $\hat{M} = |0\rangle\langle 0| \otimes |0\rangle\langle 0| \otimes \hat{I}$, at the end of this circuit, using Equation (16), and steps discussed in Section 3.1, the real part of the off-diagonal matrix element $\langle \mathbf{n}'|\hat{h}_s|\mathbf{n}\rangle$ is obtained. The imaginary part is determined under same steps, while an additional phase gate is applied to the last ancillary qubit, similar to the situation in Figure 1b.

In terms of Pauli strings, the value of $\langle\psi|\hat{M}|\psi\rangle$ is obtained from the expectations $\langle\psi|\hat{Z}_{N+2}|\psi\rangle$, $\langle\psi|\hat{Z}_{N+1}|\psi\rangle$, and $\langle\psi|\langle\hat{Z}_{N+2} \otimes \hat{Z}_{N+1}|\psi\rangle$, similar to Equation (14).

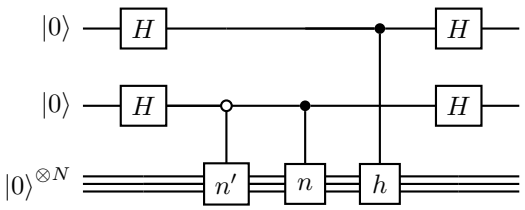

Figure 2. Quantum circuit for indirect measurement of the *real* and *imaginary* parts of an arbitrary element $\langle \mathbf{n}'|\hat{h}_s|\mathbf{n}\rangle$, for a given Pauli string operator $\hat{h}_s$. Only controlled one-qubit gates are used. The first control qubit from the top is used for the measurement of the operator $\hat{h}_s$. The second control is to prepare the quantum state of the target qubits.

Finally, using the state preparation and measurements outlined through Sections 3.1 and 3.2, all the $N_s \times N_s$ matrix elements of the effective Hamiltonian in Equation (7) can be evaluated, by repeating the execution of the quantum circuits as discussed in Figures 1 and 2, for all the possible combinations of a chosen set of $\{|\mathbf{n}\rangle\}$ bases.

Note that the approach for evaluating the *real* and *imaginary* parts of a matrix element is similar to the interference method introduced in ref. [10], with the difference being that our approach uses an ancillary qubit in order to realize the interference.

3.3. Preparing the Computational Basis

The computational basis set $\mathcal{S} = \{|\mathbf{n}\rangle\}$ with $N_s << 2^N$, needs to be specified in practice. These bases serve as the row and columns of $\hat{H}_{eff}$ in Equation (7). The process

and motivation for how to choose this set should be based on the underlying nature and physics of the problem.

In theory, one established approach to approximate the ground states of quantum many-body systems is mean-field theory [26]. In this approach, the true ground state is constructed by perturbing a reference mean-field quantum state. The quantum chemistry field has established theories and techniques for treating such problems. One particularly successful theory and numerical method is coupled cluster (CC), typically referred to as the gold-standard in computational quantum chemistry [27]. In CC, one assumes a wave-function ansatz

$$|\psi\rangle \quad = \quad e^{\hat{T}}|\mathbf{0}\rangle, \tag{17}$$

for the ground state. Here, $|\mathbf{0}\rangle$ is a reference quantum state (e.g., Hartree-Fock) and is considered to be anti-symmetric under exchange of two fermions. The operator $\hat{T} = \hat{T}_1 + \hat{T}_2 + \cdots$ is a sum over different possible excitation operators with respect to the reference state. Typically, the set of excitation operators in $\hat{T}$ includes single and double terms (i.e., CCSD), which enables a series representation of the Taylor expansion of $e^{\hat{T}}$, but high-order terms can also be added. The coefficients for the excitation operators inside $\hat{T}$ are determined by variational methods; that is, by minimizing the expectation of the Hamiltonian with respect to the ansatz [27].

Since the exponential operator in the CC ansatz, Equation (17), is non-unitary, it cannot be directly implemented on gate-based quantum computers, where gates correspond to unitary operators. Thus, a unitary version of the CC ansatz has been introduced and is known as Unitary Coupled Cluster (UCC) [15,28]. Ideally, the implementation of UCC ansatz should be constructed such that the number of gates is minimized so that the circuit depth does not exhaust the current coherence times of NISQ devices. As a result of the this concern, hardware efficient anstaz have been proposed [6] as a substitute.

In the numerical demonstration of this work (see Section 4), we consider a simplified ansatz for the ground state as:

$$\begin{aligned} |\psi\rangle \quad &= \quad c_0|\mathbf{0}\rangle \\ &+ \quad \sum_{i\nu} c_{i\nu} a_i^\dagger a_\nu |\mathbf{0}\rangle \\ &+ \quad \sum_{ij\nu\beta} c_{ij\nu\beta} a_i^\dagger a_j^\dagger a_\nu a_\beta |\mathbf{0}\rangle \\ &+ \quad \cdots, \end{aligned} \tag{18}$$

where $i, j, \ldots$ refer to the unoccupied levels, and $\nu, \beta, \ldots$, refer to occupied levels with respect to single (S), double (D), and higher order excitation operators. The ansatz in Equation (18) implies that the true many-body ground state is a superposition of the reference state $|\mathbf{0}\rangle$ and all possible S $\{a_i^\dagger a_\nu|\mathbf{0}\rangle\}$, D $\{a_i^\dagger a_j^\dagger a_\nu a_\beta|\mathbf{0}\rangle\}$, up-to $\hat{T}_n|\mathbf{0}\rangle$ excitations, where n in $\hat{T}_n$ is finite and independent of N.

In particular, assuming that it is possible to truncate the series at some low-excitation level, such as the D or triples (T), the number of eigenstates in the expansion of the above ansatz remains a polynomial function in N.

Taking the ansatz in Equation (18), we specify the set $\mathcal{S}$ in the following way. (1) Pick a computational basis as the reference quantum state, that is $|\mathbf{0}\rangle = |\mathbf{n_{int}}\rangle$. (2) Identify computational bases corresponding to a finite number of excitations, such as S and D. These are $N_s << 2^N$ bases and polynomial function in N.

In step (1), we identify the initial computational basis $|\mathbf{n_{int}}\rangle$ by minimizing the $\langle\mathbf{n_{int}}|\hat{H}|\mathbf{n_{int}}\rangle$, in which, for example, a classical Monte Carlo process from spin lattice models [29] can be used. This computational basis is essentially the qubits' configuration that has the lowest energy expectation. Since this step is a classical one, it is performed effectively even for a large number of qubits.

In step (2), once the state $|\mathbf{n_{int}}\rangle$ is determined, one can rearrange the configuration of the qubits by swapping 1's and 0's within the state $|\mathbf{n_{int}}\rangle$. The swapping is done so that the configurations corresponding to S, D, up-to $\hat{T}_n$ are fully realized. The energy expectation corresponding to these configurations (the diagonal elements in the H_{eff}) are stored on a classical register. The final result is obtained among the set of configurations whereby N_s of are the lowest energies; these are the configurations that are selected. The above steps are demonstrated numerically which is discussed in the next section (see Section 4).

4. Numerical Demonstration: LiH and BeH_2

The application of the methodology discussed in Section 3 is focused on BeH_2 and LiH molecules due to thier relatively small number of electrons and molecular orbital footprint. The number of electrons in BeH_2 and LiH is six and four, respectively. The single-electron molecular spin-orbitals in the second quantized Hamiltonian are constructed using the minimal atomic STO-3G basis set [2,6]. For BeH_2, there are a total of 14 spin-orbital, thus corresponding to 14 qubits; LiH contains 12 spin orbitals and, hence, 12 qubits. For the purpose of measuring the matrix elements of the effective Hamiltonian, Equation (7), one additional ancillary qubit is required, as illustrated in the quantum circuits shown in Figure 1. Therefore, the total number of qubits for the simulation of BeH_2 and LiH is 15 and 13, respectively.

To obtain the coefficients in the Hamiltonian of Equation (1)—more specifically as defined in Equations (2) and (3)—we make use of the Psi4 quantum chemistry package [30]. The second quantized Hamiltonian is further transfomed onto a set of Pauli strings and their corresponding weights, Equation (1), via JW transform using OpenFermion package [31].

In order to construct the potential energy surface for each inter-nuclear distance, R, the steps indicated in the previous paragraph are repeated. The distance R corresponds to the bond length between Be–H or Li–H in a given molecule; both LiH and BeH_2 are linear molecules. We note that these calculations are assuming the total Hamiltonian can be represented using the Born-Oppenheimer approximation, where the dynamics of the core nuclei are neglected. This is standard practice in quantum chemistry calculations [26]; thus, at every distance R, the nuclear-nuclear repulsion energy is treated classically and is added to the Hamiltonian as a constant.

For every distance R, a set of computational bases is chosen. This set includes the basis with the lowest energy expectation (the reference configuration) and computational bases that correspond to the low-order excitations (i.e., S, D, etc.) with respect to the reference configuration. In the case of BeH_2, we construct the effective Hamiltonian matrix by keeping the S, D, and T excitations; thus, the total number of computational bases for BeH_2 is $N_s = 1588$. The low dimension of the effective Hamiltonian matrix makes it possible to diagonalize the matrix on a classical computer using standard numerical techniques [32]. Thus, the lowest energies, including the ground state energy, are obtained at every R. The results for this process are shown in Figure 3.

Figure 3a shows the ground state energy, as well as a few low-lying excited states, for BeH_2 of the effective Hamiltonian. The exact energies are given by the dashed curves in Figure 3a. In Figure 3b, the difference between the exact and obtained ground state energy is shown. An error within the hatched area indicates results that are within chemical accuracy. Chemical accuracy is typically identified as $\sim 5 \times 10^{-3}$ Hatrees. Figure 3c shows the same energy difference for all other excited-state energies. The same process is done for LiH where only S and D configurations are used. The total number of permutations of 4 fermions (495) is reduced to $N_s = 200$, and the results are shown in Figure 4.

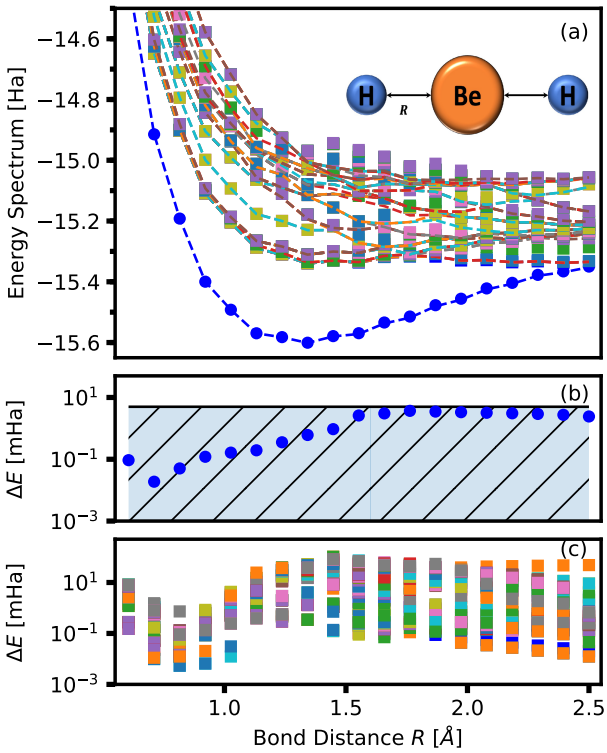

Figure 3. (**a**) The calculated binding curve of BeH_2 for the ground state and several excited states demonstrating the application of the method described in this work. (**b**) The difference between the ground state energies obtained from diagonalization of the exact and the effective Hamiltonian along with the chemical accuracy line, and (**c**) is energy difference for the obtained excited state spectra within the effective model and exact diagonalization.

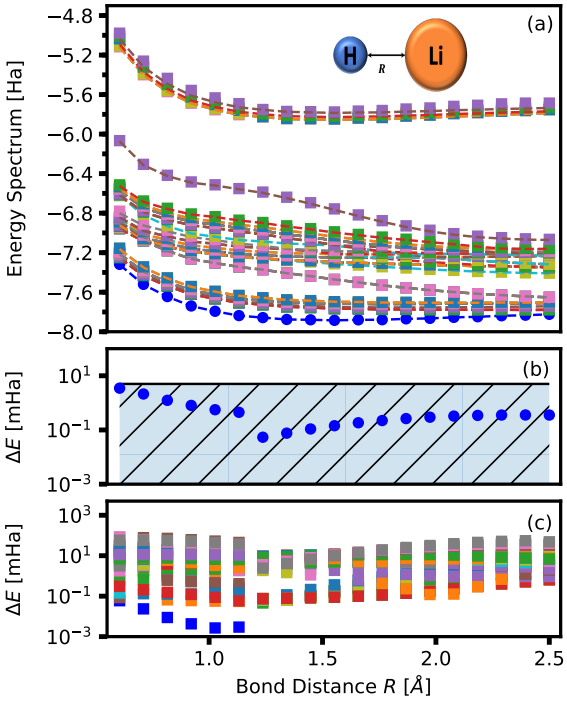

Figure 4. Similar result as shown in Figure 3 but for LiH. (**a**) Shows ground state and excited states and (**b**),(**c**) indicate energy differences compared to exact diagonalization.

The total number of configurations can be approximated by the highest excitation considered. For n-electron excitation, the number of configurations is $\binom{N_F}{n}\binom{N-N_F}{n} < N^{2n}$. Thus, the total number of configurations is less than $1 + \cdots + N^{2n} = \mathcal{O}(N^{2n})$ when $N \gg 1$. Of course, this argument is valid as long as n can be assumed to be finite and independent of the size of the system N or the number of electrons N_F. Under these assumptions, the dimensions of the effective Hamiltonian, H_{eff}, remains polynomial if one replaces the minimal STO-3G with the extended atomic basis.

Density of States

Knowledge of density of states (DOS) can be important in analyzing the thermodynamic behaviour of a system at finite temperature and in the analysis of transition states important in chemical reactions [33]. One advantage of the method proposed in this paper is the insights provided into the low-energy spectrum of the quantum system, more precisely, the degeneracy of the energy levels. To illustrate this, in Figure 5, the unnormalized DOS of the LiH obtained via the effective Hamiltonian is compared with the exact density, which shows qualitatively good agreement.

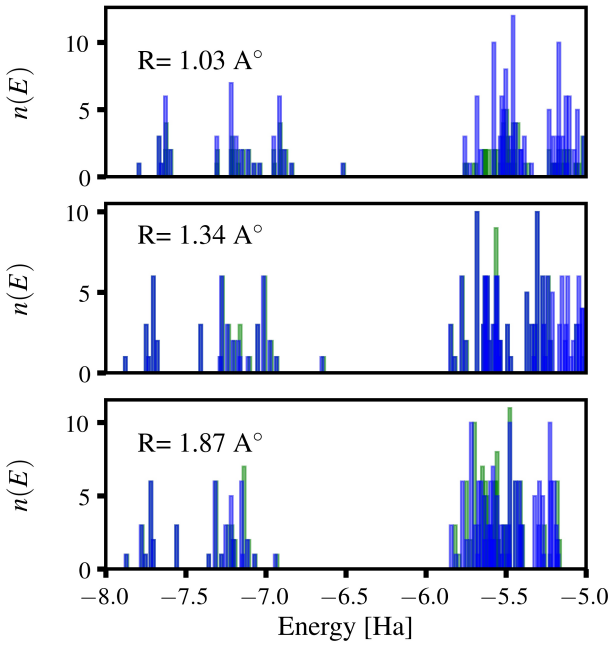

Figure 5. The unnormalizaed density of states for LiH at different binding distances. The blue fill indicates the exact, and the green fill indicates simulated.

5. Hardware Demonstration: H_2

In this section, we demonstrate the feasibility of the hybrid quantum-classical approach discussed in this paper on a IBMQ hardware device. Specifically, we calculate the eigenenergy spectrum of H_2 molecule using STO-3G minimal basis-set.

Within STO-3G basis set, the total number of spin-orbitals for H_2 is four. In contrast to the numerical demonstration, where the computational basis was prepared using the UCC ansatz, here, we employ the complete computational basis with conserved number of electrons for H_2 ($N_F = 2$). The number of computational basis set with conserved electron number, is $N_s = 6$, and the bases are:

$$\begin{aligned}\{|n_0, n_1, n_2, n_3\rangle\} = \quad & \{|1100\rangle, |1010\rangle, |1001\rangle \\ & |0110\rangle, |0101\rangle, |0011\rangle\}. \end{aligned} \tag{19}$$

The number of bases is not further reduced; that is, the effective Hamiltonian constructed here is equal to the full Hamiltonian within the $N_F = 2$ electron number. The above

set can be interpreted as the collection of all the S and D exciations, as introduced in Section 3.3, above a classical configuration, such as $|1100\rangle$.

The Hamiltonian of the problem, stated as a weighted sum of Pauli string operators, as in Equation (4), has a total of fifteen operators, which can be grouped as:

$$\begin{aligned} G_1 \quad = \quad & \{IIII,\, ZIII,\, IZII,\, IIZI,\, IIIZ,\, ZZII, \\ & ZIZI,\, ZIIZ, IZZI, IZIZ,\, IIZZ\} \end{aligned} \tag{20}$$

and

$$G_2 = \{YXXY,\, XXYY,\, YYXX,\, XYYX\}. \tag{21}$$

Here, a Pauli string operator, such as $ZIII$, is a shorthand for $\hat{Z}_1 \otimes \hat{I}_2 \otimes \hat{I}_3 \otimes \hat{I}_4$, as introduced in Equation (5).

Our goal is to use the quantum hardware to evaluate the values for $\langle \mathbf{n}|\hat{h}_s|\mathbf{n}'\rangle$, where $\hat{h}_s$ belongs to G_1 or G_2, and $|\mathbf{n}\rangle$ and $|\mathbf{n}'\rangle$ can be any of the bases listed in Equation (19).

Note that this task is not a difficult one for a classical computer. However, the objective of the paper and hardware demonstration is to establish a hybrid quantum-classical computational scheme in which the quantum processor performs some of the computational tasks. In the simulations of this paper, the task is the evaluation of the phase associated with the exchange of fermions; since $\langle \mathbf{n}|\hat{h}_s|\mathbf{n}'\rangle$ can be understood as exchanging fermions on $|\mathbf{n}\rangle$ via the operator $\hat{h}_s$, and to arrive at $|\mathbf{n}'\rangle$. The output can only take discrete values of ± 1, $\pm i$, and 0.

In each group G_1 and G_2, Pauli string operators commute and, thus, theoretically, can be measured simultaneously. However, in order to perform simultaneous measurement, one needs to adjust the computational bases, by applying further quantum gates on the target qubits. The appended measurement circuit further increases the circuit depth [34]. Thus, practically, the simultaneous measurement may not be advantageous, and, in contrast, induces further noise and decoherence on NISQ devices. Nevertheless, for G_1, no further circuit depth is required, as they are all measured in the z-basis.

We can further reduce the quantum coprocessor computational load by excluding circuits containing terms that are classically efficient to compute. In Equations (20) and (21), the operators in G_1 do not contribute to off-diagonal matrix element of the Hamiltonian, while operators in G_2 contribute *only* to the off-diagonal matrix elements. This information is used to reduce the essential number of circuits to be run on the hardware.

The evaluation of an element $\langle \mathbf{n}|\hat{h}_s|\mathbf{n}'\rangle$ is performed by assigning an appropriate circuit, as introduced in Section 3.1, to a quantum coprocessor. In this work, we make use of the IBMQ cloud open devices.

Once a circuit is loaded onto a quantum coprocessor, each circuit is executed a several times. The number of times a circuit is run is referred to as the number of shots. In this work, each circuit was executed for a total of 8000 shots. At each run, the qubits are measured, and the collection of the realized configurations is used to evaluate value of $\langle \mathbf{n}|\hat{h}_s|\mathbf{n}'\rangle$.

The preparation of the circuits is performed using the transpile and assemble routines available in the IBM Qiskit API [35], which enables collating individual circuits, corresponding to the diagonal and off-diagonal terms, to prepare each circuit to run as a single job on a target IBMQ device. In this work, we make use of the IBMQ 5-qubit Valencia hardware [17]. The number of circuits—for both real and imaginary parts separately—after the transpile and assemble routines for the diagonal and off-diagonal terms corresponds to 66 and 60 circuits, respectively. The execution timings for the IBMQ QASM simulator range between 0.21–1.5 s and for the IBMQ Valencia 5 qubit device 274–298 s with 8000 shots per circuit. Due to the limited number of qubits available on this processor, direct measurement is used, that is by measuring all the qubits at the end of the circuit.

As a sanity check, we first use IBMQ QASM simulator [36] to perform all steps involved as outlined in Section 3. The calculations are shown in Figure 6a. The results

perfectly match the exact values as expected. Furthermore, in Figure 6b the off-diagonal terms in the Hamiltonian are evaluated using IBMQ Valencia device, while the diagonal elements are evaluated using the IBMQ QASM simulator. In both cases, upon diagonalization of the obtained Hamiltonian, the energy spectrum is in good agreement with the exact values. We observe in Figure 6b that there is a slight lifting of the double degeneracy of H_2, which we associate to the device noise. This is due to the occurance of non-zero values in the measured off-diagonal terms when in fact the exact value should be zero.

Finally, all the matrix elements, that is, diagonal and off-diagonal elements, are evaluated using IBMQ Valencia device. The results are shown in Figure 7a, which was done with and without measurement error mitigation. The use of measurement error mitigation marginally improves the results. The discrepancy between the exact and hardware values, without and with measurement error mitigation, are shown in 7b,c.

The effect of noise is ubiquitous in current quantum hardware and is inherently complex and difficult to characterize. However, the result of noise due to the measurement process can be mitigated to some degree by using a calibration matrix [35]. The resulting calibration matrix is then used to reduce errors of subsequent circuit measurements. The application of measurement error mitigation is demonstrated in Figure 7a with beneficial impact on error shown in Figure 7c.

The calculations in Figure 7, that is construction of the effective Hamiltonian, $\hat{H}_{eff}$, are performed through five independent IBMQ job submissions. Each time the energy-surface is slightly different, which can be associated to the inherent device errors and perhaps low number of shots used. The error bars in Figure 7b,c indicate the min/max range in errors of the five different calculation.

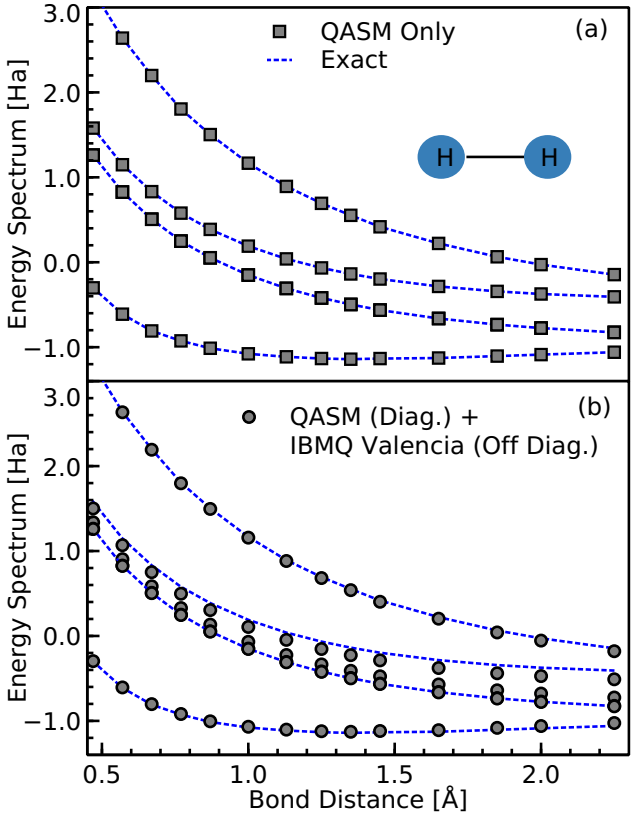

Figure 6. The binding curves for H_2 using a (**a**) noiseless QASM simulator to obtain all Pauli terms and (**b**) a noiseless QASM simulator to evaluate diagonal Pauli terms and the IBMQ Valencia 5-qubit device to measure off-diagonal terms.

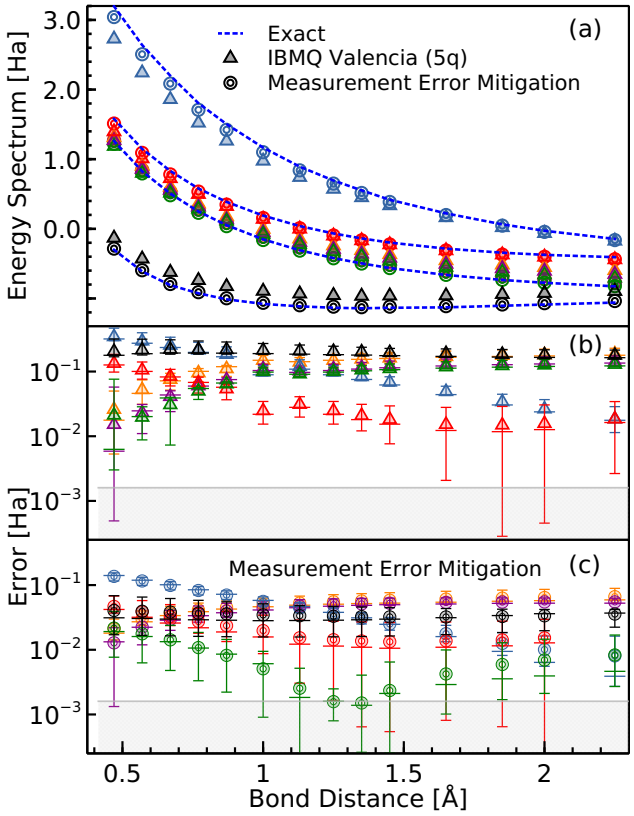

Figure 7. The complete hardware calculation using the IBMQ Valencia 5-qubit device. The lowest value shown in (**a**) for 5 distinct hardware runs where 8000 shots is used. The absolute error between exact and hardware results is shown in (**b**), where symbol indicates the mean and error-bars min/max amongst the 5 runs. (**c**) The same as (**b**) but with measurement error mitigation for the target hardware. The semi-opaque region in (**b**),(**c**) indicates chemical accuracy limit.

6. Discussion and Summary

Recently an abundance of Variational Quantum Algorithms (VQA) have been introduced to solve electronic quantum many-body problems on NISQ devices [3–5,8–11,28]. These VQA proposals mostly rely on optimization of parametric circuits. In this paper, we demonstrate that an alternative approach exists, specifically for quantum chemistry problems, which does not require an optimization procedure and parametric ansatz. In this approach, the quantum hardware is used only to prepare a many-body quantum state and to efficiently measure the expectation values of certain target observables with respect to this quantum state. From the output measurements, one can construct what we refer to as an effective Hamiltonian matrix, $\hat{H}_{eff}$. Upon diagonalization of $\hat{H}_{eff}$ using classical eigen-decomposition numerical methods one obtains the ground state and low-lying excited states of the system.

The approach introduced in this paper is particularly suitable for NISQ devices where short quantum circuit depth is essential due to lack of error-correction protocols on these devices. An additional important aspect of this approach is that it provides access to the low-lying energy spectra of the system and not just the ground state in comparison with the original VQE process.

In the context of VQE and VQE-type algorithms, several attempts have been made to extend the variational approach to excited states [10,11,37–40]. Quantum subspace expansion [41,42], for example, constructs a set of non-orthogonal bases out of an optimized ansatz, and performs post-processing to obtain excited states. Deflation techniques as described in ref. [11], constructs a pseudo-Hamiltonian in which the ground state is excluded and orthogonality is enforced through regularization. Successful examples are introduced for some low-lying excited states of LiH [8]. In all these previous works, optimization of a

parametric ansatz is required and, therefore, necessitates an enormous number of quantum circuit executions and sampling.

The approach introduced in this paper is similar to multistate contracted VQE (MC-VQE) in ref. [10]. The main difference is the application of VQE: MC-VQE is obviously a VQE-type algorithm, our approach is distinct in that it does not require a parametric circuit or variational procedure for optimization. In addition, our method differs since it uses supporting quantum circuit resources, i.e., ancilla qubits, in order to perform interference and measurement that is different from the quantum circuit in ref. [43] and its generalization in ref. [10].

An extension of our approach to VQE type algorithm is possible. This can be done by appending a set of parametric gates that act only on the target qubits to the circuits in Figure 1. Let us denote this part of the circuit with $U(\theta)$, where θ stands for a set of parameters. Then, it can be verified that, given θ, the final matrix element obtained from the circuit after measurement (see Equation (2), for example) becomes $\langle \mathbf{n}|U^{\dagger}(\theta)\hat{H}U(\theta)|\mathbf{n}'\rangle$, compared to $\langle \mathbf{n}|\hat{H}|\mathbf{n}'\rangle$. The appended parametric circuit $U(\theta)$ allows one to project the Hamiltonian onto $\mathcal{S}(\theta) = \{U(\theta)|\mathbf{n}\rangle\}$, for a given θ. This means the $N_s \times N_s$ effective Hamiltonian is now parametric and depends on the value(s) of θ. The optimal parameter(s) are then obtained by minimizing the ground-state energy of the effective Hamiltonian matrix. The reference state $\{U(\theta)|\mathbf{n}\rangle\}$ can be regarded as the contracted reference states introduced in ref. [10].

One possible limitation of the circuits shown in Figure 1 is the execution of two-qubit gates corresponding to control operations over n-qubits (i.e., series of CNOT gates). For NISQ devices with hardware-restricted qubit connectivity, this may require a number of SWAP gate operations and, therefore, can increase the circuit depth and subsequent error rates [44,45]. In essence, the implementation of the circuits described in this paper will depend on the ability to limit circuit depth and associated error rates by NISQ hardware circuit optimization (i.e., scheduling). However, significant improvements in qubit connectivity of various modalities (e.g., ion traps) [22,46] or optimizing quantum circuits against decoherence [47,48] may blunt this concern.

Author Contributions: P.J. and S.B. contributed equally to this work. All authors have read and agreed to the published version of the manuscript.

Funding: The ideas and methodology discussed in Section 3 have been supported by General Atomics internal R&D funds. Their application towards quantum chemistry problems as discussed in Sections 4 and 5 is based upon work supported by the U.S. Department of Energy, Office of Science, Office of Fusion Energy Sciences, under Award Number DE-SC0020249. *Disclaimer*: A portion of this report was prepared as an account of work sponsored by an agency of the United States Government. Neither the United States Government nor any agency thereof, nor any of their employees, makes any warranty, express or implied, or assumes any legal liability or responsibility for the accuracy, completeness, or usefulness of any information, apparatus, product, or process disclosed, or represents that its use would not infringe privately owned rights. Reference herein to any specific commercial product, process, or service by trade name, trademark, manufacturer, or otherwise does not necessarily constitute or imply its endorsement, recommendation, or favoring by the United States Government or any agency thereof. The views and opinions of authors expressed herein do not necessarily state or reflect those of the United States Government or any agency thereof.

Data Availability Statement: The data and scripts that support the findings of this study are available from the corresponding author upon reasonable request.

Acknowledgments: We thank Mark Kostuk for his guidance and management as PI under this grant. Additionally, we thank David P. Schissel for feedback and guidance at General Atomics. We also greatly thank Yuri Alexeev and Martin Suchara from Argonne National Laboratory for fruitful discussion and feedback. Circuit diagrams are rendered using the LaTeX Quantikz package [49], numerical scripts utilize the Python SciPy package [32], and 2D plots are generated with the Python matplotlib package [50]. We acknowledge use of the IBMQ for this work. The views expressed are those of the authors and do not reflect the official policy or position of IBM or the IBMQ team.

Conflicts of Interest: The authors declare no conflict of interest.

References

1. Preskill, J. Quantum Computing in the NISQ era and beyond. *Quantum* **2018**, *2*, 79, doi:10.22331/q-2018-08-06-79.
2. McArdle, S.; Endo, S.; Aspuru-Guzik, A.; Benjamin, S.C.; Yuan, X. Quantum computational chemistry. *Rev. Mod. Phys.* **2020**, *92*, 015003, doi:10.1103/RevModPhys.92.015003.
3. Yuan, X.; Endo, S.; Zhao, Q.; Li, Y.; Benjamin, S.C. Theory of variational quantum simulation. *Quantum* **2019**, *3*, 191, doi:10.22331/q-2019-10-07-191.
4. Peruzzo, A.; McClean, J.; Shadbolt, P.; Yung, M.H.; Zhou, X.Q.; Love, P.J.; Aspuru-Guzik, A.; O'brien, J.L. A variational eigenvalue solver on a photonic quantum processor. *Nat. Commun.* **2014**, *5*, 4213, doi:10.1038/ncomms5213.
5. McClean, J.R.; Romero, J.; Babbush, R.; Aspuru-Guzik, A. The theory of variational hybrid quantum-classical algorithms. *New J. Phys.* **2016**, *18*, 023023, doi:10.1088/1367-2630/18/2/023023.
6. Kandala, A.; Mezzacapo, A.; Temme, K.; Takita, M.; Brink, M.; Chow, J.M.; Gambetta, J.M. Hardware-efficient variational quantum eigensolver for small molecules and quantum magnets. *Nature* **2017**, *549*, 242–246, doi:10.1038/nature23879.
7. Barkoutsos, P.K.; Gonthier, J.F.; Sokolov, I.; Moll, N.; Salis, G.; Fuhrer, A.; Ganzhorn, M.; Egger, D.J.; Troyer, M.; Mezzacapo, A.; et al. Quantum algorithms for electronic structure calculations: Particle-hole Hamiltonian and optimized wave-function expansions. *Phys. Rev. A* **2018**, *98*, 022322, doi:10.1103/PhysRevA.98.022322.
8. Jones, T.; Endo, S.; McArdle, S.; Yuan, X.; Benjamin, S.C. Variational quantum algorithms for discovering Hamiltonian spectra. *Phys. Rev. A* **2019**, *99*, 062304, doi:10.1103/PhysRevA.99.062304.
9. Nakanishi, K.M.; Mitarai, K.; Fujii, K. Subspace-search variational quantum eigensolver for excited states. *Phys. Rev. Res.* **2019**, *1*, 033062, doi:10.1103/PhysRevResearch.1.033062.
10. Parrish, R.M.; Hohenstein, E.G.; McMahon, P.L.; Martínez, T.J. Quantum Computation of Electronic Transitions Using a Variational Quantum Eigensolver. *Phys. Rev. Lett.* **2019**, *122*, 230401, doi:10.1103/PhysRevLett.122.230401.
11. Higgott, O.; Wang, D.; Brierley, S. Variational Quantum Computation of Excited States. *Quantum* **2019**, *3*, 156, doi:10.22331/q-2019-07-01-156.
12. Jouzdani, P.; Bringuier, S.; Kostuk, M. A Method of Determining Excited-States for Quantum Computation. *arXiv* **2019**, arXiv:1908.05238.
13. McClean, J.R.; Boixo, S.; Smelyanskiy, V.N.; Babbush, R.; Neven, H. Barren plateaus in quantum neural network training landscapes. *Nat. Commun.* **2018**, *9*, 1–6, doi:10.1038/s41467-018-07090-4.
14. Parrish, R.M.; Iosue, J.T.; Ozaeta, A.; McMahon, P.L. A Jacobi Diagonalization and Anderson Acceleration Algorithm For Variational Quantum Algorithm Parameter Optimization. *arXiv* **2019**, arXiv:1904.03206.
15. Romero, J.; Babbush, R.; McClean, J.R.; Hempel, C.; Love, P.; Aspuru-Guzik, A. Strategies for quantum computing molecular energies using the unitary coupled cluster ansatz. *arXiv* **2017**, arXiv:1701.02691.
16. Herasymenko, Y.; O'Brien, T.E. A diagrammatic approach to variational quantum ansatz construction. *arXiv* **2019**, arXiv:1907.081576.
17. IBM-Q team. IBM-Q 5 Qubit Valencia Backend, Specification v1.3.1. 2020. Available online: https://quantum-computing.ibm.com (accessed on 15 October 2020)
18. Reine, S.; Helgaker, T.; Lindh, R. Multi-electron integrals. *Wiley Interdiscip. Rev. Comput. Mol. Sci.* **2012**, *2*, 290–303.
19. Fradkin, E. Jordan-Wigner transformation for quantum-spin systems in two dimensions and fractional statistics. *Phys. Rev. Lett.* **1989**, *63*, 322, doi:10.1103/PhysRevLett.63.322.
20. Nielsen, M.A.; Chuang, I. *Quantum Computation and Quantum Information*; American Cambridge University Press: Cambridge, UK, 2016.
21. Steudtner, M.; Wehner, S. Quantum codes for quantum simulation of fermions on a square lattice of qubits. *Phys. Rev. A* **2019**, *99*, 022308, doi:10.1103/PhysRevA.99.022308.
22. Wright, K.; Beck, K.M.; Debnath, S.; Amini, J.M.; Nam, Y.; Grzesiak, N.; Chen, J.S.; Pisenti, N.C.; Chmielewski, M.; Collins, C.; et al. Benchmarking an 11-qubit quantum computer. *Nat. Commun.* **2019**, *10*, doi:10.1038/s41467-019-13534-2.
23. Knill, E.; Ortiz, G.; Somma, R.D. Optimal quantum measurements of expectation values of observables. *Phys. Rev. A* **2007**, *75*, 012328, doi:10.1103/PhysRevA.75.012328.
24. Dobšíček, M.; Johansson, G.; Shumeiko, V.; Wendin, G. Arbitrary accuracy iterative quantum phase estimation algorithm using a single ancillary qubit: A two-qubit benchmark. *Phys. Rev. A* **2007**, *76*, 030306, doi:10.1103/PhysRevA.76.030306.
25. Mitarai, K.; Fujii, K. Methodology for replacing indirect measurements with direct measurements. *Phys. Rev. Res.* **2019**, *1*, 013006, doi:10.1103/PhysRevResearch.1.013006.
26. Jensen, F. *Introduction to Computational Chemistry*; John Wiley & Sons: Hoboken, NJ, USA, 2017.
27. Bartlett, R.J.; Musiał, M. Coupled-cluster theory in quantum chemistry. *Rev. Mod. Phys.* **2007**, *79*, 291.
28. Wecker, D.; Hastings, M.B.; Troyer, M. Progress towards practical quantum variational algorithms. *Phys. Rev. A* **2015**, *92*, 042303, doi:10.1103/PhysRevA.92.042303.
29. Janke, W. Monte Carlo Simulations of Spin Systems. In *Computational Physics: Selected Methods Simple Exercises Serious Applications*; Springer: Berlin/Heidelberg, Germany, 1996; pp. 10–43, doi:10.1007/978-3-642-85238-1_3.

30. Parrish, R.M.; Burns, L.A.; Smith, D.G.A.; Simmonett, A.C.; DePrince, A.E.; Hohenstein, E.G.; Bozkaya, U.; Sokolov, A.Y.; Di Remigio, R.; Richard, R.M.; et al. Psi4 1.1: An Open-Source Electronic Structure Program Emphasizing Automation, Advanced Libraries, and Interoperability. *J. Chem. Theory Comput.* **2017**, *13*, 3185–3197, doi:10.1021/acs.jctc.7b00174.
31. McClean, J.R.; Sung, K.J.; Kivlichan, I.D.; Cao, Y.; Dai, C.; Fried, E.S.; Gidney, C.; Gimby, B.; Gokhale, P.; Häner, T.; et al. OpenFermion: The Electronic Structure Package for Quantum Computers. *arXiv* **2017**, arXiv:1710.07629.
32. Virtanen, P.; Gommers, R.; Oliphant, T.E.; Haberland, M.; Reddy, T.; Cournapeau, D.; Burovski, E.; Peterson, P.; Weckesser, W.; Bright, J.; et al. SciPy 1.0: Fundamental Algorithms for Scientific Computing in Python. *Nat. Methods* **2020**, doi:10.1038/s41592-019-0686-2.
33. Truhlar, D.G.; Garrett, B.C.; Klippenstein, S.J. Current status of transition-state theory. *J. Phys. Chem.* **1996**, *100*, 12771–12800, doi:10.1021/jp953748q.
34. Gui, K.; Tomesh, T.; Gokhale, P.; Shi, Y.; Chong, F.T.; Martonosi, M.; Suchara, M. Term Grouping and Travelling Salesperson for Digital Quantum Simulation. *arXiv* **2020**, arXiv:2001.05983.
35. Qiskit team. Qiskit: An Open-source Framework for Quantum Computing. 2019. Available online: https://zenodo.org/record/2562111#.YBYhA3kRVPY (accessed on 15 October 2020).
36. IBM-Q Team. IBM-Q QASM Backend, Specification v0.1.547, 2020. Available online: https://quantum-computing.ibm.com (accessed on 15 October 2020).
37. Tilly, J.; Jones, G.; Chen, H.; Wossnig, L.; Grant, E. Computation of molecular excited states on IBMQ using a Discriminative Variational Quantum Eigensolver. *arXiv* **2020**, arXiv:2001.04941.
38. Santagati, R.; Wang, J.; Gentile, A.A.; Paesani, S.; Wiebe, N.; McClean, J.R.; Morley-Short, S.; Shadbolt, P.J.; Bonneau, D.; Silverstone, J.W.; et al. Witnessing eigenstates for quantum simulation of Hamiltonian spectra. *Sci. Adv.* **2018**, *4*, eaap9646.
39. McArdle, S.; Jones, T.; Endo, S.; Li, Y.; Benjamin, S.C.; Yuan, X. Variational ansatz-based quantum simulation of imaginary time evolution. *Npj Quantum Inf.* **2019**, *5*, doi:10.1038/s41534-019-0187-2.
40. Somma, R.D. Quantum eigenvalue estimation via time series analysis. *arXiv* **2019**, arXiv:1907.11748.
41. McClean, J.R.; Kimchi-Schwartz, M.E.; Carter, J.; de Jong, W.A. Hybrid quantum-classical hierarchy for mitigation of decoherence and determination of excited states. *Phys. Rev. A* **2017**, *95*, doi:10.1103/physreva.95.042308.
42. Colless, J.I.; Ramasesh, V.V.; Dahlen, D.; Blok, M.S.; Kimchi-Schwartz, M.E.; McClean, J.R.; Carter, J.; de Jong, W.A.; Siddiqi, I. Computation of Molecular Spectra on a Quantum Processor with an Error-Resilient Algorithm. *Phys. Rev. X* **2018**, *8*, 011021, doi:10.1103/PhysRevX.8.011021.
43. Diker, F. Deterministic construction of arbitrary *W* states with quadratically increasing number of two-qubit gates. *arXiv* **2016**, arXiv:1606.0929.
44. Venturelli, D.; Do, M.; Rieffel, E.; Frank, J. Compiling quantum circuits to realistic hardware architectures using temporal planners. *Quantum Sci. Technol.* **2018**, *3*, 025004, doi:10.1088/2058-9565/aaa331.
45. Nash, B.; Gheorghiu, V.; Mosca, M. Quantum circuit optimizations for NISQ architectures. *Quantum Sci. Technol.* **2020**, *5*, 025010, doi:10.1088/2058-9565/ab79b1.
46. Hazra, S.; Salunkhe, K.V.; Bhattacharjee, A.; Bothara, G.; Kundu, S.; Roy, T.; Patankar, M.P.; Vijay, R. Engineering cross resonance interaction in multi-modal quantum circuits. *Appl. Phys. Lett.* **2020**, *116*, 152601, doi:10.1063/1.5143440.
47. Zhang, Y.; Deng, H.; Li, Q.; Song, H.; Nie, L. Optimizing Quantum Programs against Decoherence: Delaying Qubits into Quantum Superposition. In Proceedings of the 2019 International Symposium on Theoretical Aspects of Software Engineering (TASE), Guilin, China, 29–31 July 2019; pp. 184–191.
48. Holmes, A.; Jokar, M.R.; Pasandi, G.; Ding, Y.; Pedram, M.; Chong, F.T. NISQ+: Boosting quantum computing power by approximating quantum error correction. *arXiv* **2020**, arXiv:2004.04794.
49. Kay, A. Quantikz. 2019. Available online: https://royalholloway.figshare.com/articles/dataset/Quantikz/7000520/4 (accessed on 15 October 2020).
50. Hunter, J.D. Matplotlib: A 2D graphics environment. *Comput. Sci. Eng.* **2007**, *9*, 90–95, doi:10.1109/MCSE.2007.55.